Available online at www.sciencedirect.com
ScienceDirect
Ceramics International 37 (2011) 1873–1877
CERAMICS INTERNATIONAL
www.elsevier.com/locate/ceramint

Effects of Al_2O_3 on the properties and densification of 8YSZ after pulsed current activated sintering

In-Jin Shon *, Kwon-il Na, In-Yong Ko, Jeong-Hwan Park

Division of Advanced Materials Engineering and the Research Center of Advanced Materials Development, College of Engineering, Chonbuk National University, 664-14 Deokjin-dong 1-ga, Deokjin-gu, Jeonju, Jeonbuk 561-756, South Korea

Received 13 January 2011; accepted 8 February 2011
Available online 15 February 2011

Abstract

Dense 8YSZ was subjected to pulsed current activated sintering (PCAS) within 1 min of 8YSZ nanopowder preparation using a co-precipitation method. Sintering was accomplished by combining a pulsed current and mechanical pressure. Highly dense 8YSZ with a relative density of up to 99% was produced under simultaneous application of a pressure of 80 MPa and the pulsed current. The effects of the addition of Al_2O_3 on the sintering behavior, mechanical properties, and ionic conductivities of 8YSZ were investigated.

Keywords: C. Mechanical properties; C. Ionic conductivity; Pulsed current activated sintering; 8YSZ; Densification

1. Introduction

Solid oxide fuel cells (SOFCs) systems are very attractive because of their high efficiency and very low pollutant emissions. Yttria-stabilized zirconia (YSZ) has been extensively used as an electrolyte in solid oxide fuel cells (SOFCs) because of its attractive properties which include a high oxygen ion conductivity and low electronic conductivity at high temperature, stability in both oxidizing and reducing atmospheres, and a relatively low cost [1,2]. In addition to these advantages, their high fracture strength and toughness, excellent thermal conductivity, and good thermal expansion compatibility with other cell components make these materials suitable for fabrication as self-supported electrolyte plates for use in planar SOFC systems. Such systems have higher volumetric power densities than those of alternative tubular SOFC systems.

Cubic zirconia stabilized with 8 mol% yttria (8YSZ) is commonly used as the electrolyte material in SOFCs due to its high ionic conductivity at high operating temperature. However, the main drawbacks of zirconia-based materials are that they are difficult to fully densify at temperatures less than 1500 °C, and they cannot easily form a nanostructure due to the fast grain growth during conventional sintering [3]. It has been reported that some transition metal oxides such as MnO_2, Co_3O_4, and Fe_2O_3 are very effective sintering aids for the densification of metal oxides [4,5].

In order to achieve a high ionic conductivity, the material must be prepared in a dense and uniform state with a well controlled stoichiometry. Recent studies concerning stabilized zirconia have shown that the ionic conductivity may be influenced by the microstructure and grain size. The total ionic conductivity of 8YSZ is mainly influenced by the grain boundaries rather than by the grains [6]. A larger number of grain boundaries and the existence of porosity lead to a greater resistivity in fine-grained samples. Additionally, the reduction in grain size also changes the mechanical properties and the sintering behaviors of nanocrystalline materials [7,8]. The sintering temperature of nanocrystalline zirconia is about 400–500 °C lower than that of the corresponding microcrystalline material [9].

When conventional sintering processes are used to sinter nano-sized zirconia powders, concomitant grain growth leads to the destruction of the nanostructure. This has led to increased interest in consolidation methods in which grain growth can be eliminated or significantly reduced. To accomplish this, rapid sintering methods have been widely used to sinter nano-sized powders. The most obvious advantage of rapid sintering is that the fast heating and cooling rates and the short dwell time lead

* Corresponding author. Tel.: +82 63 2381; fax: +82 63 270 2386.
E-mail addresses: ijshon@chonbuk.ac.kr, ijshon@jbnu.ac.kr (I.-J. Shon).

0272-8842/$36.00
doi:10.1016/j.ceramint.2011.02.002

to the bypass of low temperature, non-densifying mass transport (e.g., surface diffusion) [10,11]. However, conventional rapid heating can lead to temperature gradients and thus differential densification (non-uniform microstructures), low density, or specimen cracking. To overcome these issues, other rapid sintering techniques such as the pulsed current activated sintering method [12] have been developed.

In this work, we report the fabrication of nanosized 8YSZ powders and the sintering properties of Al_2O_3-containing 8YSZ materials using a pulsed current activated sintering (PCAS) method under high pressure. We also investigated the effects of Fe_2O_3 on the sintering behavior, mechanical properties and ionic conductivity of the 8YSZ electrolyte.

2. Experimental procedure

Nanopowders of 8YSZ and Al_2O_3 were produced via a co-precipitation method using diluted ammonia as a precipitant. High purity (>99.99%) $Y(NO_3)_3{\cdot}6H_2O$, $ZrO(NO_3)_2{\cdot}6H_2O$, and Al $(NO_3)_3{\cdot}9H_2O$ reagents were used as the starting materials. 8YSZ and Al_2O_3 powders were milled in a universal mill with a ball:powder weight ratio of 6:1. Milling was performed in polyethylene bottles using zirconia balls and was carried out at a horizontal rotation velocity of 250 rpm for 24 h.

The powder was placed in a graphite die (outer diameter of 45 mm, inner diameter of 20 mm, and a height of 40 mm) and then introduced into the pulsed current activated sintering system made by Eltek (South Korea), as shown schematically in reference [12]. The PCAS apparatus consisted of an 18 V, 2800 A-DC power supply which provided a pulsed current with a 20 μs on-time and a 10 μs off-time through the sample and die and a 50 kN uniaxial press. The system was evacuated, a uniaxial pressure of 80 MPa was applied, and the DC current was then activated. Sample shrinkage was monitored in real-time using a linear gauge to measure the vertical displacement, and the temperatures were measured with a pyrometer focused on the surface of the graphite die. Depending on the heating rate, the electrical and thermal conductivities of the compact and its relative density, there was a difference in the temperatures between the surface and the center of the sample. The sample was sintered at 1200 °C at a heating rate of about 1000 °C/min. At the end of the process, the current was turned off and the sample was allowed to cool to room temperature. The process was carried out under vacuum at a pressure of 40 mTorr.

The relative densities of the synthesized samples were measured using the Archimedes method. Microstructural information was obtained from the thermally etched product samples. Compositional and microstructural analyses of the products were carried out using X-ray diffraction (XRD) and scanning electron microscopy (SEM) evaluations with energy dispersive X-ray analysis (EDAX). After polishing with SiC paper, Pt was coated onto both sides of the sintered pellets. The ionic conductivity was measured from 350 to 500 °C in air using a two-probe impedance spectroscopy (Zahner IM6, Germany) method in the frequency range of 100 mHz to 3 MHz with a voltage amplitude of 50 mV.

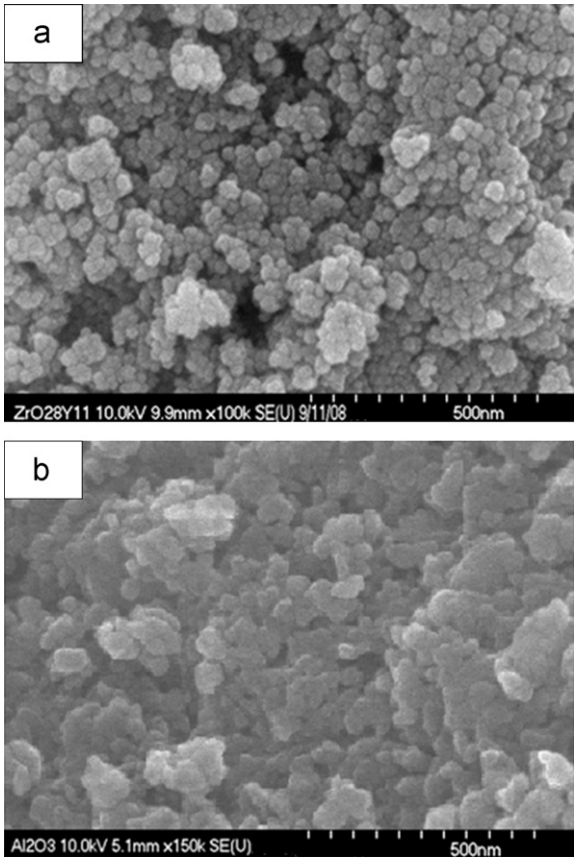

Fig. 1. FE-SEM images of (a) 8YSZ powder and (b) Al_2O_3 powder synthesized using a co-precipitation method.

3. Results and discussion

3.1. Powder characterization

Fig. 1 shows FE-SEM images of the precipitated 8YSZ powder and Al_2O_3 powder calcined at 600 °C for 1 h in air. The powder sizes of 8YSZ and Al_2O_3 were less than 50 nm. The XRD results (Fig. 2) showed that all of the peaks for the powder

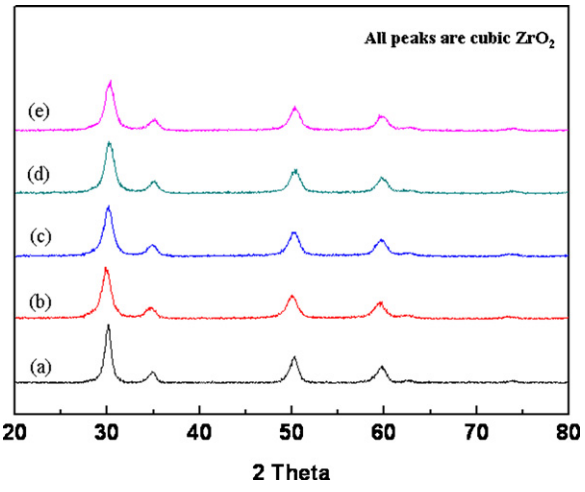

Fig. 2. X-ray diffraction patterns of 8YSZ–Al_2O_3 powders synthesized using the co-precipitation method with Al_2O_3 contents of (a) 0 mol%, (b) 0.5 mol%, (c) 1 mol%, (d) 2 mol%, and (e) 3 mol%.

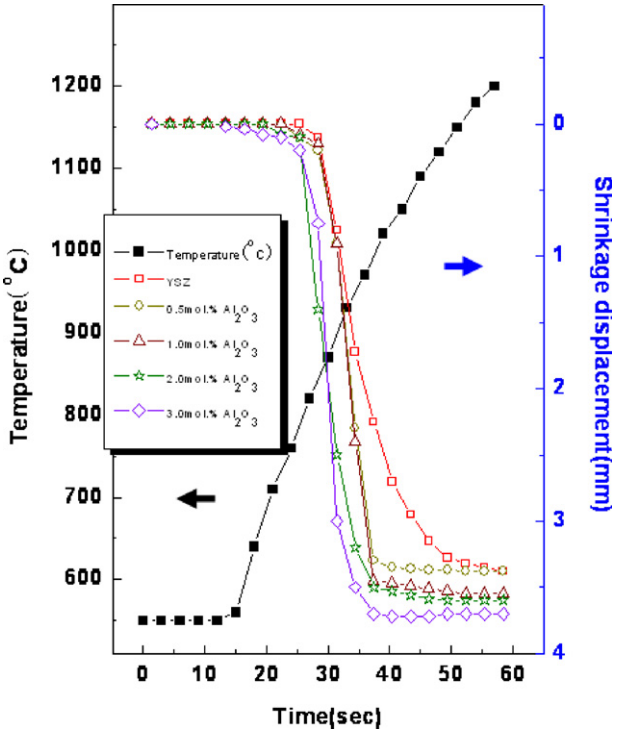

Fig. 3. Variations in temperature and shrinkage displacement with heating time during PCAS of 8YSZ containing Al_2O_3.

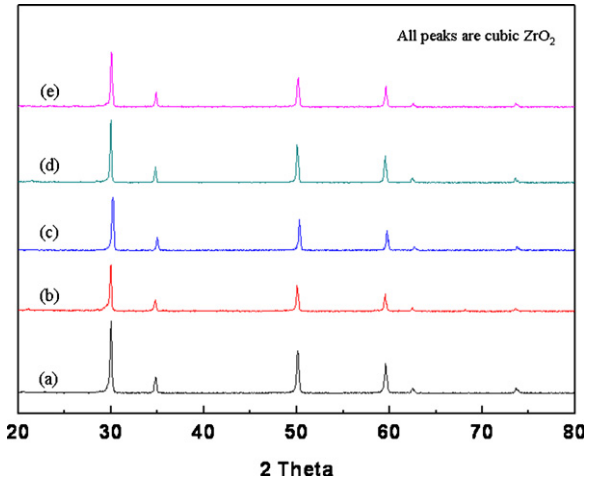

Fig. 4. X-ray diffraction patterns of sintered 8YSZ with Al_2O_3 contents of (a) 0 mol%, (b) 0.5 mol%, (c) 1 mol%, (d) 2 mol%, and (e) 3 mol%.

calcined at 600 °C corresponded to the fluorite structure of ZrO_2 (PDF card number: 03-0640). The lattice parameter of the sample calcined at 600 °C was determined to be 0.5100 nm using the least square refinement method. This value agrees well with the theoretical lattice parameter of the fluorite structure of ZrO_2 (theoretical lattice parameter,

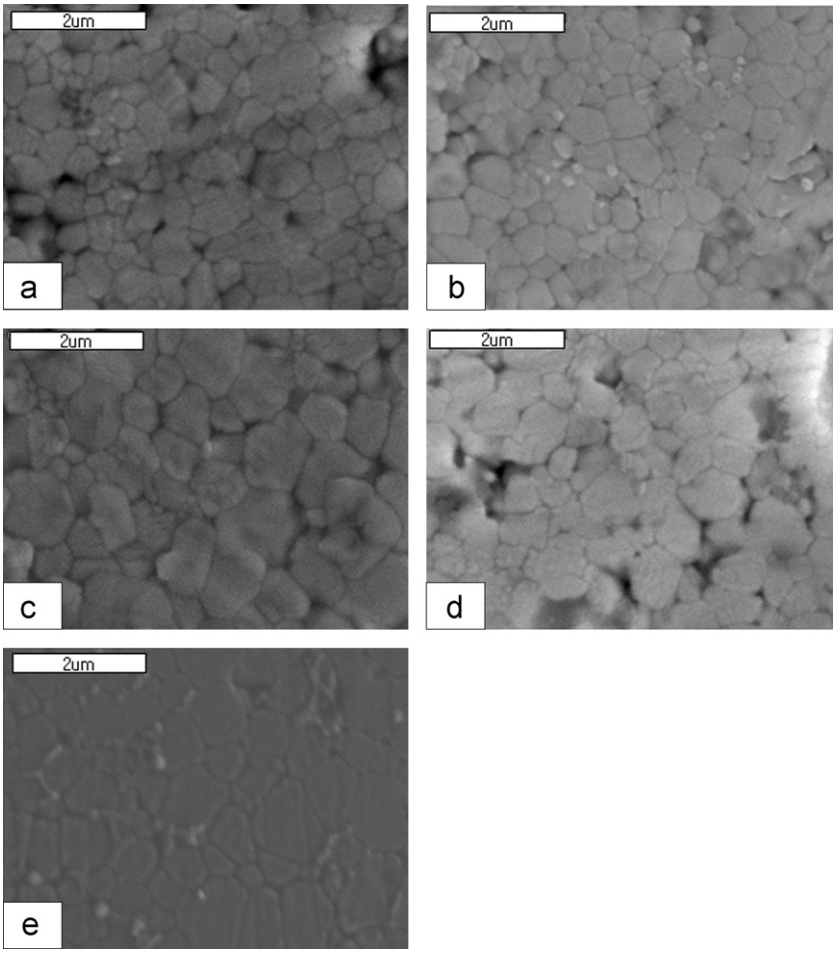

Fig. 5. SEM images of the thermally etched 8YSZ with Al_2O_3 contents of (a) 0 mol%, (b) 0.5 mol%, (c) 1 mol%, (d) 2 mol%, and (e) 3 mol%.

a = 0.5103 nm). There was a very slight difference between the calculated and theoretical lattice parameter due to the substitution of Zr^{4+} with Y^{3+} in the fluorite structure of ZrO_2.

3.2. Densification behavior of 8YSZ

The variations in the shrinkage displacement and temperature of the surface of the graphite die with heating time during the processing of 8YSZ doped with different concentrations of Al_2O_3 under a pressure of 80 MPa are shown in Fig. 3. As the pulsed current was applied, the shrinkage displacement increased with temperature. In addition, Al_2O_3 doping was extremely effective in promoting the densification of 8YSZ when exceeding a dopant concentration of 0.5 mol%. The addition of Al_2O_3 to the ZrO_2 system led to the formation of oxygen vacancies due to charge compensation. It was expected that these oxygen vacancies enhanced the densification rate and promoted grain boundary mobility. Moreover, the addition of Al_2O_3 may induce a large distortion in the surrounding lattice because Al^{3+} ions are much smaller than Zr^{4+} ions. It was also expected that the lattice distortion would promote grain boundary mobility due to the effect of the severely undersized dopant [13].

Fig. 4 shows the XRD patterns of the specimens sintered with various Al_2O_3 contents. Only the fluorite structure of the ZrO_2 peaks was detected. Fig. 5 shows the SEM images of 8YSZ sintered with 0, 0.5, 1, 2, and 3 mol% Al_2O_3. The average sizes of the grains determined with the linear intercept method were about 500, 700, 900, 900, and 900 nm for 8YSZ with additions of 0, 0.5, 1, 2, and 3 mol% produced by PCAS at 1200 °C, respectively. The relative densities of 8YSZ with additions of 0, 0.5, 1, 2, and 3 mol% were 96.5, 98, 99, 97, and 97%, respectively.

3.3. Ionic conductivity of 8YSZ

Fig. 6 shows the grain interior and grain boundary conductivities of 8YSZ with Al_2O_3. The grain boundary conductivity was lower than the grain interior conductivity. In previous studies, it was assumed that the grain boundary resistance was the result of a siliceous phase [14]. Recently, however, it has been reported that the grain boundary conductivity of samples with impurity-free grain boundaries is still about two orders of magnitude lower than that of the bulk or grain interior [15]. It has also been suggested that oxygen vacancy depletion can be affected by dopant ion segregation [16]. There was no great difference in the conductivities of the grain interior and grain boundary in 8YSZ with Al_2O_3.

The ionic conductivity was fit as a function of temperature by applying the Arrhenius law:

$$\sigma = \left(\frac{\sigma_o}{T}\right)\exp\left(\frac{-E_a}{k_B T}\right), \quad (1)$$

where E_a is the activation energy for ionic migration, k_B is the Boltzmann constant, and σ_o is the pre-exponential factor, a constant related to the carrier density (in this case, oxide vacancies). Fig. 7 shows the Arrhenius plots of the grain interior and grain boundary conductivities of 8YSZ with Al_2O_3 content; there were no significant differences in the activation energies according to Al_2O_3 content. The activation energies of the grain interior and grain boundary of 8YSZ calculated from Eq. (1) were 0.10 eV and 1.15 eV, respectively.

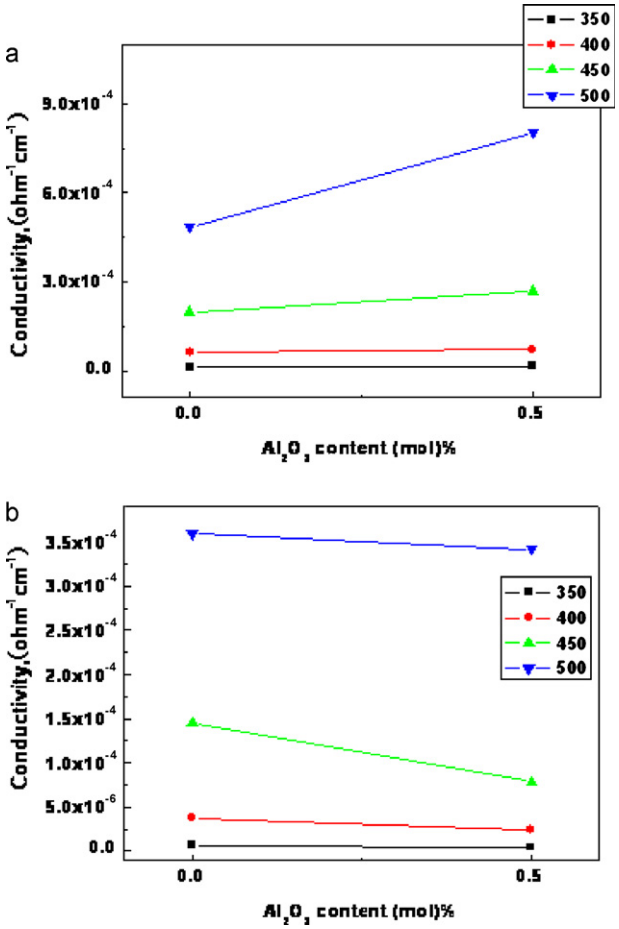

Fig. 6. (a) Grain interior and (b) grain boundary conductivities of 8YSZ and 8YSZ with 0.5 mol% Al_2O_3 at various temperatures.

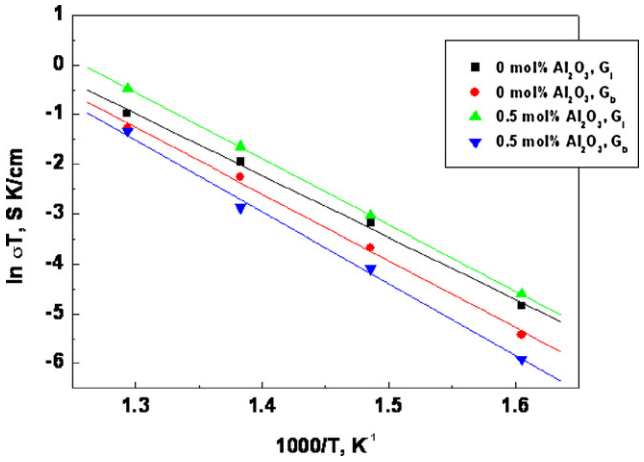

Fig. 7. Arrhenius plots of the grain interior (G_i) and grain boundary conductivities (G_b) of 8YSZ and 8YSZ with 0.5 mol% Al_2O_3.

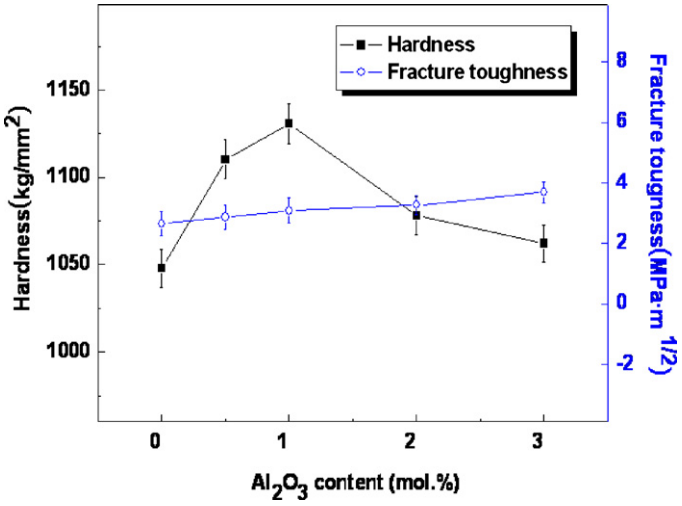

Fig. 8. The hardness and fracture toughness values of 8YSZ with various Al_2O_3 contents.

3.4. Mechanical properties of 8YSZ oxides

To investigate the mechanical properties of the samples, Vickers hardness and fracture toughness measurements were performed on polished sections of the 8YSZ ceramics using a 1 Kg_f load and a 15 s dwell time. The mechanical properties were investigated on samples densified under a pressure of 80 MPa with a heating rate of 1000 °C/min up to 1200 °C. Indentation with sufficiently large loads produced radial cracks emanating from the corners of the indent. The fracture toughness was calculated from the cracks produced in the indentations under the large loads. The lengths of these cracks allowed for the estimation of the fracture toughness of the materials by applying the following expression [17]:

$$K_{IC} = 0.204\left(\frac{c}{a}\right)^{-3/2} \times H_v a^{1/2}, \quad (2)$$

where c is the trace length of the crack measured from the center of the indentation, a is half of the average length of two indent diagonals, and H_v is the hardness.

The mechanical property results are shown in Fig. 8. There were no significant differences in the fracture toughness with Al_2O_3 content. However, the hardness gradually increased with Al_2O_3 addition up to 1 mol% and then decreased with further addition of Al_2O_3 due to the relative density. The hardness and fracture toughness of 8YSZ sintered at 1200 °C were about 1050 kg/mm^2 and 3 MPa m$^{1/2}$, respectively.

4. Summary

In this study, nanopowders of 8YSZ and Al_2O_3 were fabricated using a co-precipitation method. Using the pulsed current activated sintering (PCAS) method, the densification of 8YSZ nanopowder was performed. The relative density of 8YSZ under an applied pressure of 80 MPa and a pulsed current was 96.5%. The relative density increased with addition of Al_2O_3, while the grain interior and grain boundary conductivities of 8YSZ did not vary greatly. The grain boundary conductivity was smaller than the grain bulk conductivity, and the activation energies of the grain interior and grain boundary of 8YSZ were 0.10 eV and 1.15 eV, respectively.

References

[1] J. Maier, Nano-sized mixed conductors (aspects of nano-ionics part III), Solid State Ionics 148 (2002) 367–374.
[2] J. Schoonman, Nanoionics, Solid State Ionics 157 (2003) 319–326.
[3] S. Tekeli, The flexural strength, fracture toughness, hardness and densification behavior of various amount of Al_2O_3-doped 8YSCZ/Al_2O_3 composites used as an electrolyte for solid oxide fuel cell, Mater. Des. 27 (2006) 230–235.
[4] T.S Zhang, J. Ma, Y.J. Leng, S.H. Chan, P. Hing, J.A. Kilner, Effect of transition metal oxides on densification and electrical properties of Si-containing $Ce_{0.8}Gd_{0.2}O_{2-\delta}$ ceramics, Solid State Ionics 168 (2004) 187–195.
[5] C. Kleinlogel, L.J. Gauckler, Sintering and properties of nanosized ceria solid solutions, Solid State Ionics 135 (2000) 567–573.
[6] R. Ramamoorthy, D. Sundararaman, S. Ramasamy, Ionic conductivity studies of ultrafine-grained yattria stabilized zirconia polymorphs, Solid State Ionics 123 (1999) 271–278.
[7] M.J. Verkerk, B.J. Middelhuis, A.J. Burgraaf, Effect of grain boundaries on the conductivity of high-purity ZrO_2–Y_2O_3 ceramics, Solid State Ionics 6 (1982) 159–165.
[8] H.C. Kim, I.J. Shon, J.E. Garay, Z.A. Munir, Consolidation and properties of binderless sub-micron tungsten carbide by field-activated sintering, Int. J. Refract. Met. Hard Mater. 22 (2004) 257–264.
[9] M. Yoshimura, T. Ohji, M. Sando, K. Niihara, Rapid rate sintering of nano-grained ZrO_2-based composites using pulsed electric current sintering method, J. Mater. Sci. Lett. 17 (1998) 1389–1391.
[10] D.J. Chen, M.J. Mayo, Rapid rate sintering of nanocrystalline ZrO_2-3 mol% Y_2O_3, J. Am. Ceram. Soc. 79 (1996) 906–910.
[11] D.J. Chen, M.J. Mayo, Nanocrystalline intermetallic compounds prepared by mechanical alloying, NanoStruct. Mater. 2 (1993) 469–475.
[12] I.-Y. Ko, J.-H. Park, K.-S. Nam, I.-J. Shon, Rapid consolidation of nanocrystalline $NbSi_2$–Si_3N_4 composites by pulsed current activated combustion synthesis, Met. Mater. Inter. 16 (2010) 393–398.
[13] P.L. Chen, I.W. Chen, Grain growth in CeO_2: dopant effects, defect mechanism, and solute drag, J. Am. Ceram. Soc. 79 (1996) 1793–1800.
[14] M.C Martin, M.L. Mecartney, Grain boundary ionic conductivity of yttrium stabilized zirconia as a function of silica content and grain size, Solid State Ionics 161 (2003) 67–79.
[15] M. Aoki, Y.M. Chiang, I. Kosacki, J.R. Lee, H. Tuller, Y. Liu, Solute segregation and grain-boundary impedance in high-purity stabilized zirconia, J. Am. Ceram. Soc. 79 (1996) 1169–1180.
[16] X. Guo, Size dependent grain-boundary conductivity in doped zirconia, Comput. Mater. Sci. 20 (2001) 168–176.
[17] N. Koichi, Evaluation of K_{IC} of brittle solids by the indentation method with low crack-to-indent ratios, J. Mater. Sci. Lett. 1 (1982) 13–16.